PHYSICAL REVIEW B **84**, 174120 (2011)

Terahertz and infrared spectroscopic evidence of phonon-paramagnon coupling in hexagonal piezomagnetic $YMnO_3$

C. Kadlec,[1] V. Goian,[1] K. Z. Rushchanskii,[2] P. Kužel,[1] M. Ležaić,[2] K. Kohn,[3] R. V. Pisarev,[4] and S. Kamba[1,*]

[1]*Institute of Physics ASCR, Na Slovance 2, 182 21 Prague 8, Czech Republic*

[2]*Peter Grünberg Institut, Forschungszentrum Jülich GmbH, 52425 Jülich and JARA-FIT, Germany*

[3]*Waseda University, Department of Physics, Tokyo 169-8555, Japan*

[4]*Ioffe Physical-Technical Institute, Russian Academy of Sciences, 194021 St. Petersburg, Russia*

(Received 31 August 2011; revised manuscript received 4 November 2011; published 22 November 2011)

Terahertz and far-infrared electric and magnetic responses of hexagonal piezomagnetic $YMnO_3$ single crystals are investigated. Antiferromagnetic resonance is observed in the spectra of magnetic permeability μ_a [$\mathbf{H}(\omega)$ oriented within the hexagonal plane] below the Néel temperature T_N. This excitation softens from 41 to 32 cm^{-1} upon heating and finally disappears above T_N. An additional weak and heavily-damped excitation is seen in the spectra of complex dielectric permittivity ε_c within the same frequency range. This excitation contributes to the dielectric spectra in both antiferromagnetic and paramagnetic phases. Its oscillator strength significantly increases upon heating toward room temperature, thus providing evidence of piezomagnetic or higher-order couplings to polar phonons. Other heavily-damped dielectric excitations are detected near 100 cm^{-1} in the paramagnetic phase in both ε_c and ε_a spectra, and they exhibit similar temperature behavior. These excitations appearing in the frequency range of magnon branches well below polar phonons could remind electromagnons, however their temperature dependence is quite different. We have used density functional theory for calculating phonon dispersion branches in the whole Brillouin zone. A detailed analysis of these results and of previously published magnon dispersion branches brought us to the conclusion that the observed absorption bands stem from phonon-phonon and phonon-paramagnon differential absorption processes. The latter is enabled by strong short-range in-plane spin correlations in the paramagnetic phase.

DOI: 10.1103/PhysRevB.84.174120 PACS number(s): 75.85.+t, 78.30.−j, 63.20.D−, 75.30.Ds

I. INTRODUCTION

Spin waves (magnons) in magnetically ordered materials can be excited by the magnetic component $\mathbf{H}(\omega)$ of the electromagnetic radiation, giving rise to a resonant dispersion of magnetic permeability in the microwave or terahertz (THz) frequency region. Recently, new coupled spin-lattice excitations named electromagnons have been discovered in multiferroics, where the magnetic order coexists with the ferroelectric one.[1,2] Electromagnons are excited by the electric component $\mathbf{E}(\omega)$ of the electromagnetic radiation, therefore they can be detected in the THz dielectric permittivity spectra. Though they were theoretically predicted in 1970,[3] the first experimental confirmation appeared in 2006.[1] These excitations were mainly investigated in the rare earth (R) orthorhombic manganites $RMnO_3$ and RMn_2O_5 (for reviews see, e.g., Refs. 4–6), and in hexaferrites.[7]

Multiferroics can be roughly divided into two groups.[8–10] In the so-called type-I multiferroics, the ferroelectric (FE) order takes place both above and below the magnetic ordering temperature, and the spontaneous polarization is large. However, the coupling between magnetic and electric order parameters is weak.

A general feature of type-II multiferroic materials is that the ferroelectric phase is induced by magnetic ordering characterized by a particular type of incommensurate spiral magnetic structure. In this case, the magnetically-induced polarization is by several orders of magnitude smaller than in type-I multiferroics. However the coupling between electric and magnetic subsystems is large, and giant magnetoelectric effects are observed. The magnon dispersion branch in the incommensurate phase exhibits a minimum at the wave vector $\boldsymbol{q}_m$ corresponding to the modulation vector of the ordered spins. In contrast to the magnetic resonance (magnon at $\mathbf{q} \approx 0$) characterized by sharp spectral features, the electromagnons manifest themselves as very broad spectral bands, because their activation in the dielectric spectra is closely related to the high density of states close to the extrema of the magnon dispersion branches. Since the probing THz radiation has a long wavelength (i.e., the wave vector $\mathbf{q} \approx 0$), the electromagnons cannot be excited by a resonant single-photon absorption due to the wave vector conservation law; in this sense polar phonons should be involved in the interaction process.

An experimentally observed low-frequency electromagnon in type-II multiferroics was found to be related to the spin waves near the magnetic Brillouin zone (BZ) center with $\mathbf{q} = \mathbf{q}_m$;[4,11] or to those with $\mathbf{q} = \mathbf{q}_{BZE} - 2\mathbf{q}_m$;[12] here $\boldsymbol{q}_{BZE}$ stands for the wave vector at the BZ edge. In both cases, the low-frequency electromagnon has a similar frequency as the magnon with $q = 0$, which is expected because all these excitations are related to the same magnon branch. A high-frequency electromagnon corresponds to an excitation of the BZ-edge magnons ($\mathbf{q} = \mathbf{q}_{BZE}$) which can induce a quasiuniform modulation ($\mathbf{q} \approx 0$) of the local electric dipole moment.[11,13] As for mechanisms of the electromagnon excitations, some researchers claim that the low-frequency electromagnons are activated by the inverse Dzyaloshinskii-Moriya mechanism, while the high-frequency one is activated by the Heisenberg exchange coupling.[5,6] Other authors believe that both types of electromagnons can be explained by the Heisenberg exchange coupling.[14]

Formerly, it was assumed that the electromagnons can be activated only in type-II multiferroics due to the large

magnetoelectric coupling. Nevertheless, electromagnons were recently observed also in $BiFeO_3$,[15–17] which is the most prominent type-I multiferroic with a rather weak magnetoelectric coupling. In this context, THz dielectric spectra of multiferroics may shed new light on the nature of magnetoelectric coupling.

Hexagonal manganites $RMnO_3$ belong to the type-I multiferroics. In particular, the hexagonal $YMnO_3$ is ferroelectric below ≈1250 K[18] and the antiferromagnetic (AFM) ordering sets only below $T_N \approx 70$ K.[19,20] The magnetic symmetry is $P6_3cm$[21] and therefore the linear magnetoelectric coupling is forbidden. However, piezomagnetic and magnetoelastic couplings and higher-order magnetoelectric couplings are allowed.[22–24] The piezomagnetic coupling is characterized by a bilinear interaction between the magnetic order parameter and strain, in contrast to the magnetoelastic coupling which is proportional to the product of squared order parameter and strain.[22,25] By using the method of optical second harmonic generation,[26] the piezomagnetic coupling was observed owing to the interaction between AFM and FE domain walls in $YMnO_3$.[23,24] Switching of the FE polarization triggers a reversal of the AFM order parameter.[23,24,27] Higher order magnetoelectric coupling in $YMnO_3$ has been observed in several works. Exceptionally large atomic displacements at T_N were observed in structural studies, and they demonstrate unusually strong magnetoelastic coupling.[28] The large spin–polar-phonon coupling manifests itself by a decrease of the low-frequency permittivity[29] near T_H, which is probably caused by anomalous hardening of several infrared-active phonons.[30] Similar phonon anomalies were observed near T_N also in the Raman spectra.[31] Ultrasound measurements on a single crystal of the hexagonal $YMnO_3$ showed anomalous behavior of the elastic moduli C_{11} and C_{66} due to a strong coupling of the lattice with the in-plane exchange interaction.[32]

The AFM resonance in hexagonal $YMnO_3$ crystal was first reported in Ref. 33. More detailed THz studies of $YMnO_3$ ceramics were recently published in Ref. 34. The AFM resonance lies near 43 cm^{-1} at 4 K, and its frequency softens upon heating toward T_N, where it disappears.[33,34] Three magnon branches were discovered below T_N using inelastic neutron scattering (INS).[20,35,36] Two of them are degenerated near the BZ center, and their frequencies correspond to the above-mentioned AFM resonance. Moreover, a possible existence of magnons and short-range correlations between spins at Mn sites in paramagnetic phase were indicated by INS.[37–39] The magnetoelastic coupling manifests itself also by a strong mixing of magnons with acoustic phonons; this leads to a gap in the transverse acoustic (TA) phonon branch occurring at the frequencies and wave vectors where the uncoupled magnon and TA branches would intersect.[36] Recent polarized INS measurements revealed that the excitation detected at liquid helium temperatures near 43 cm^{-1} has a mixed character of magnetic spin wave and lattice vibration,[40] i.e., its contribution to both the magnetic permeability and the dielectric permittivity is possible.

The reported piezomagnetic, magnetoelastic, and higher-order magnetoelectric couplings in optical, acoustic, and mainly INS data stimulated our spectroscopic study of hexagonal single crystals of $YMnO_3$. In this paper, we present results on far-infrared (FIR) and THz polarized spectra in this material emphasizing interaction between magnetic, electric, and phonon subsystems. We demonstrate that strongly underdamped AFM resonance observed near ≈40 cm^{-1} contributes only to the magnetic permeability spectra below T_N. An additional broad and weak absorption band was observed in the same frequency range in the dielectric spectra both below and above T_N. In contrast to electromagnons which are typically observed only below 50 K, the oscillator strength of this excitation significantly increases upon heating when room temperature is approached. This indicates that the feature must be related to the occupation number of magnons and/or phonons. An additional absorption band with similar temperature behavior was observed also near 100 cm^{-1}. We will show that both these excitations can be explained by differential multiphonon and magnon-phonon processes.

II. EXPERIMENTAL DETAILS

The experiments were performed using a Fourier-transform infrared (FTIR) spectrometer Bruker IFS 113v and a custom-made THz time-domain spectrometer.[41] In both experiments, Optistat CF cryostats (Oxford Instruments) with polyethylene (FIR) or Mylar (THz) windows were used for measurements between 10 and 300 K. A helium-cooled bolometer operating at 1.6 K was used as a detector in the FTIR spectrometer. Principles of THz time-domain spectroscopy are explained in Ref. 42. The output of a femtosecond Ti:sapphire laser oscillator (Coherent, Mira) excites an interdigitated photoconducting switch TeraSED (Giga-Optics) to generate linearly polarized broadband THz probing pulses. A gated detection scheme based on an electro-optic sampling with a 1-mm-thick [110] ZnTe crystal permits to measure the time profile of the electric field of the transmitted THz pulse (see Ref. 41 for further details).

Hexagonal $YMnO_3$ single crystals were grown by the floating zone method.[43] Two crystal plates with lateral dimensions of $\sim 4.5 \times 5$ mm^2 and with the c axis oriented either in-plane or out-of-plane along its normal, were cut and polished to obtain highly plane-parallel samples (within ± 1 μm) with thicknesses of 1100 and 348 μm for each orientation, respectively. These crystal plates were probed using the THz and FIR beam in all possible geometries: $\mathbf{E}(\omega) \perp \mathbf{c}, \mathbf{H}(\omega) \perp \mathbf{c}$; $\mathbf{E}(\omega) \perp \mathbf{c}, \mathbf{H}(\omega) \| \mathbf{c}$; and $\mathbf{E}(\omega) \| \mathbf{c}, \mathbf{H}(\omega) \perp \mathbf{c}$. It enabled us to get access to the complex spectra of the products $\varepsilon_a \mu_a$, $\varepsilon_a \mu_c$, and $\varepsilon_c \mu_a$ as shown in Figs. 1(a), 1(b), and 1(c), respectively.

III. RESULTS

At low temperatures, the peak around 40 cm^{-1} seen in the spectra of $\varepsilon_a \mu_a$ and $\varepsilon_c \mu_a$ [Figs. 1(a) and 1(c)] but not in those of $\varepsilon_a \mu_c$ [Fig. 1(b)] is definitely due to the AFM resonance as it contributes only to the magnetic permeability μ_a. The AFM resonance vanishes above $T_N \sim 70$ K. The data shown in Fig. 1(b) allow us to assume that $\mu_c = 1$ in the THz range. This is in agreement with the magnetic order of $YMnO_3$ in the AFM phase: The spins are ordered in adjacent layers in the hexagonal plane in such a way that the magnetic resonances are not expected to be excited with $\mathbf{H} \| \mathbf{c}$. Based on this assumption, we are able to retrieve the complex values of the permeability μ_a and of the permittivity ε_c (see Fig. 2).

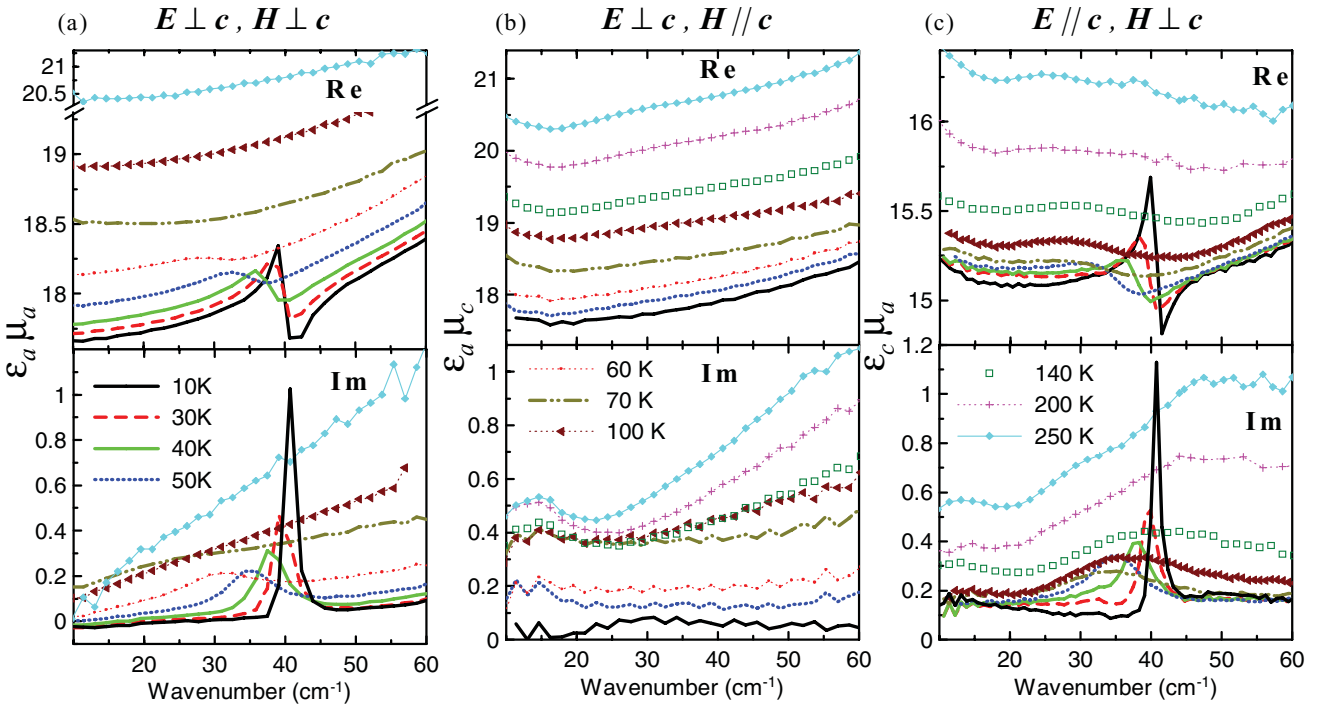

FIG. 1. (Color online) Complex THz spectra of $YMnO_3$ taken at various temperatures. The polarization of the THz beam is indicated above the plots. The resonance feature near ~40 cm^{-1} corresponds to the doubly-degenerated AFM mode contributing to the magnetic permeability μ_a spectra.

The spectra of μ_a were fitted by a damped harmonic oscillator, and the resulting AFM resonance frequency is plotted in Fig. 3; a strong softening is observed upon heating toward T_N. Similar temperature dependence was briefly published earlier,[33,34] with the magnon frequency higher by approximately 2 cm^{-1}. Besides the sharp AFM resonance line in the low-temperature μ_a spectra, one can observe a broad dielectric absorption band around 40 cm^{-1} in the ε_c spectra. This feature is detected even above T_N, where its strength remarkably increases with temperature. The presence of such a resonance in ε_c is qualitatively expected from a simple comparison of the raw data in Figs. 1(a) and 1(c). The accessible spectral range of the THz measurements for our sample is limited to ~60 cm^{-1}, therefore we have performed also FTIR transmission (up to 100 cm^{-1}) and reflectivity (up to 650 cm^{-1}) measurements for all polarizations.

An example of FTIR experimental transmittance and reflectivity spectra obtained at 120 K and their various

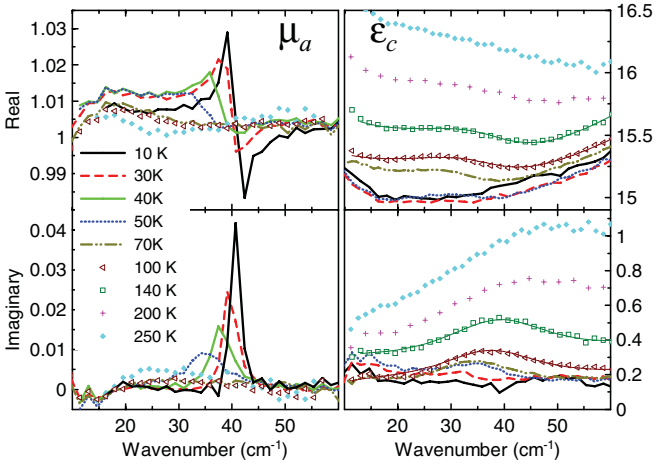

FIG. 2. (Color online) Temperature dependence of the complex permittivity ε_c and permeability μ_a spectra calculated from data plotted in Fig. 1. The solid ε_c curves at 100 and 140 K result from the oscillator fit.

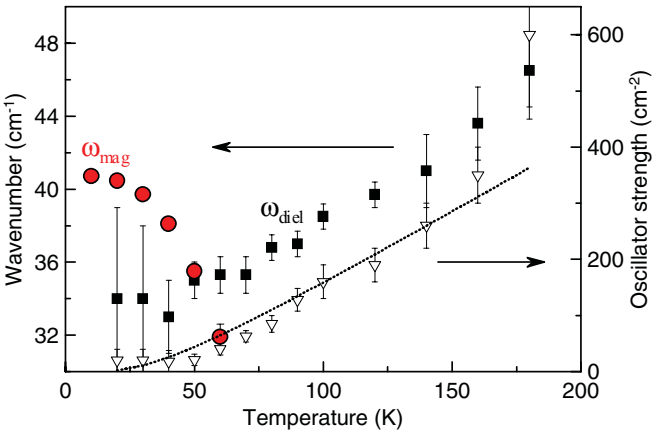

FIG. 3. (Color online) Temperature dependences of parameters of the resonances observed in magnetic μ_a and dielectric ε_c spectra. Closed circles: frequency of the AFM resonance. Solid squares and open triangles: eigenfrequency ω_{diel1} and oscillator strength $\Delta\varepsilon\omega^2_{diel1}$, respectively, of the mode observed in the dielectric spectra in Fig. 2. The dotted line shows the population increase of an energy level at 66 cm^{-1} following the Bose-Einstein statistics.

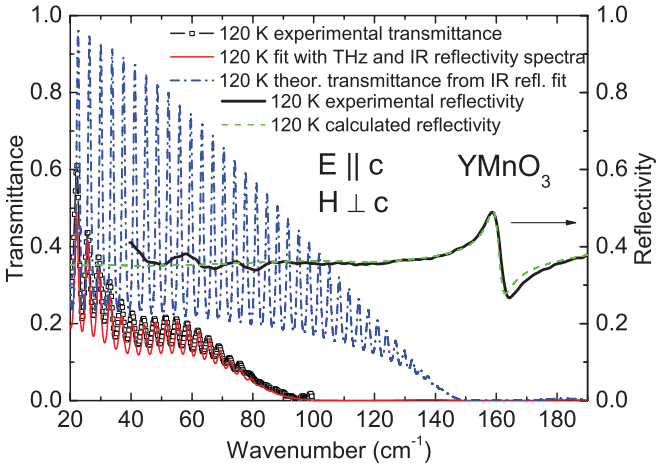

FIG. 4. (Color online) Example of the experimental FTIR transmittance and reflectivity spectra of 348-μm-thick $YMnO_3$ crystal with polarization **E**‖**c** obtained at 120 K. Dashed-dotted blue line: theoretical transmittance spectrum obtained from parameters of the FTIR reflectivity fit (without considering modes observed by THz spectroscopy); solid red line: simultaneous fit of the FTIR transmission and THz spectra. Dashed green line is the result of a fit of the reflectivity using the parameters obtained from the fit of FIR and THz transmittance. One can see that the reflectivity spectrum is not sensitive enough to detect the weak broad modes near 40 and 100 cm^{-1}. Oscillations in the experimental reflectivity spectrum observed below 80 cm^{-1} are caused by the diffraction of FIR beam on a small sample.

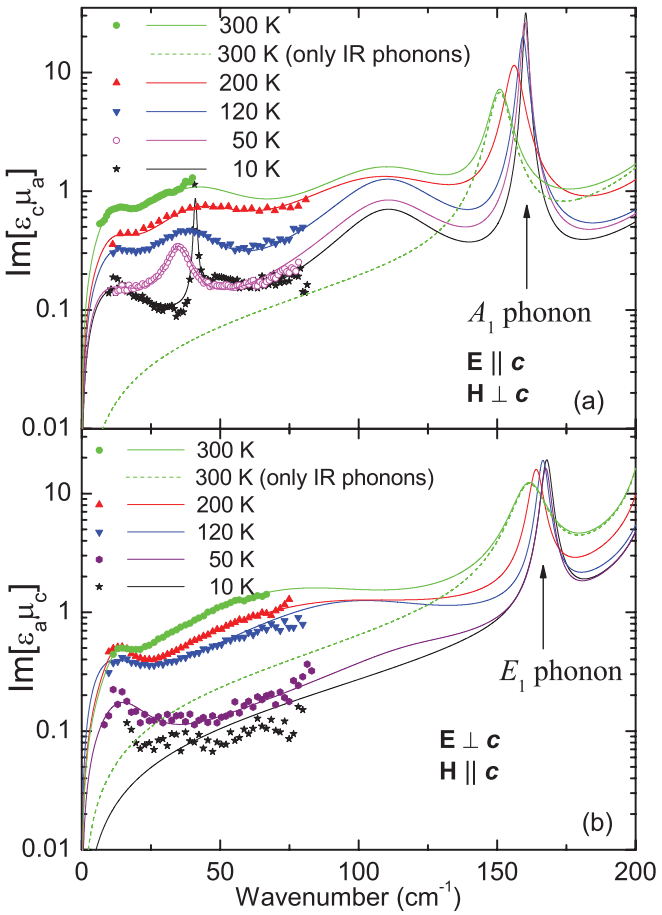

FIG. 5. (Color online) The measured THz loss spectra of $YMnO_3$ (symbols) and those obtained from the fits of FTIR transmittance and reflectivity spectra. Below $T_N = 70$ K, the spectra correspond to imaginary parts of the permittivity-permeability product. Above T_N, the spectra correspond to the dielectric losses. Polarizations of electric and magnetic components of IR or THz beams are indicated. Dashed lines are the fits of room-temperature FTIR reflectivity spectra without taking into account the IR and THz transmittance spectra. The marked peaks above 150 cm^{-1} are due to phonons; the origin of lower frequency absorption bands is discussed in the text.

fits are shown in Fig. 4. Regular oscillations observed in the transmittance spectrum are due to Fabry-Pérot interferences in the plane-parallel sample; a weak minimum near 40 cm^{-1} corresponds to the broad absorption band detected in the THz dielectric spectra (see Fig. 2). According to Ref. 30 as well as according to our FTIR reflectivity (see e.g. Fig. 4), the lowest frequency polar phonons lie above 150 cm^{-1} in both polarized **E**‖**c** and **E** ⊥ **c** spectra. Nevertheless, our simultaneous fits of the THz complex permittivity and FTIR transmittance and reflectivity data reveal several additional modes below these phonon frequencies. The relevant spectra are plotted in Fig. 5. Besides the sharp magnon line at 40 cm^{-1}, three other broad modes at roughly 10, 40, and 100 cm^{-1} were used in the fitting procedure in order to account for the measured shape of the **E**‖**c** spectra at 10 K [see Fig. 5(a)]. The additional modes remain in the spectra up to room temperature and their strength increases upon heating. Also in **E** ⊥ **c** polarized spectra, two broad modes observed near 10 and 90 cm^{-1} were used for the fits above 50 K.

The feature observed near 10 cm^{-1} in both polarized spectra could be related to low-frequency magnons[35] (cf., the low-frequency magnon branches shown in Fig. 7). However, the sensitivity and accuracy of our THz spectra below 20 cm^{-1} is limited; therefore we cannot exclude that it is only an artifact. For this reason, we will not speculate about the origin of this excitation. All other modes appearing below 150 cm^{-1} are clearly observed in the THz and/or FTIR transmittance spectra, while the FTIR reflectivity measurements are not sensitive enough to detect and resolve these weak and broad spectral features (see Fig. 4). Their origin will be discussed in the next section.

The temperature dependence of the sub-THz complex dielectric permittivity ε_a plotted in Fig. 6 for 20 cm^{-1} exhibits a pronounced drop below T_N. Such an anomaly is a typical feature of large spin-phonon coupling which occurs only in hexagonal planes of $YMnO_3$, where the spins are ordered. For that reason the anomaly is not observed in $\varepsilon_c(T)$. The AFM phase transition is accompanied by unusually large atomic displacements, which were detected by neutron diffraction;[28] for this reason the phonon frequencies change below T_N. The decrease in ε_a' and ε_a'' is mainly caused by hardening of the E_1 symmetry polar mode seen near 250 cm^{-1} in the IR reflectivity spectra with polarization **E** ⊥ **c**.[30] Fits of our IR reflectivity spectra show that the mode near 250 cm^{-1} hardens from 246 cm^{-1} (at 300 K) to 256 cm^{-1} (at 10 K) and therefore its dielectric contribution $\Delta\varepsilon$ is reduced from 9.1 (300 K) to 7.6 (10 K). This decrease of $\Delta\varepsilon$ is mainly responsible for the

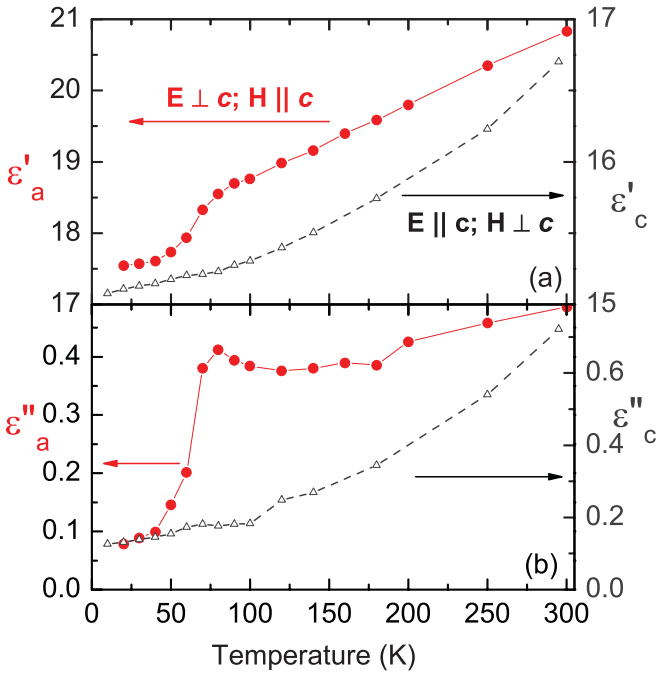

FIG. 6. (Color online) Temperature dependence of the (a) permittivity and (b) dielectric loss measured at 20 cm^{-1} with polarization $\mathbf{E} \perp \mathbf{c}$ (red solid lines) and $\mathbf{E} \parallel \mathbf{c}$ (black dashed lines).

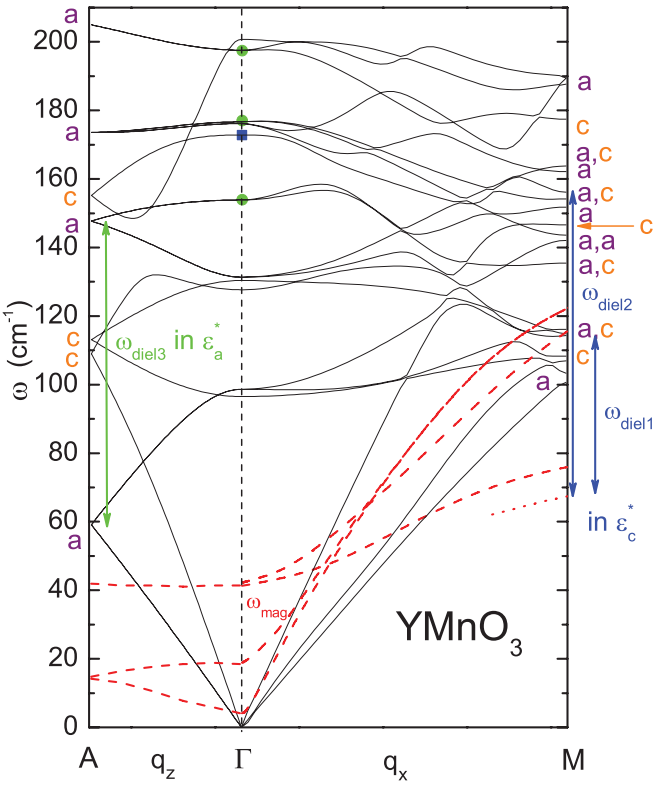

FIG. 7. (Color online) Dispersion branches of phonons (theoretical; black solid lines) and magnons (experimental[35] at 7 K; red dashed lines). The red-dotted line indicates the presumable dispersion of the paramagnon near the M point. The symbols shown at the BZ edges indicate the polarization of the phonons at the BZ boundary: a and c stand for phonons polarized within the hexagonal plane and in the perpendicular direction, respectively. In the Γ-point, the E_1 and A_1 phonons observed experimentally[30] are marked by green and blue points, respectively; other modes are silent. Blue arrows with assignment ω_{diel1} and ω_{diel2} indicate phonon-paramagnon excitations observed in the dielectric loss spectra of ε_c''. Green arrow marked as ω_{diel3} indicates a broad multiphonon absorption observed in the ε_a'' loss spectra (see Fig. 5).

change of the permittivity $\varepsilon_a'(T)$ seen in Fig. 6. Hardening of other modes brings a minor contribution to the decrease of $\varepsilon_a'(T)$ upon cooling. Similar temperature dependence of ε_a' was observed also in the radio-frequency region[29] providing evidence of the absence of dielectric dispersion below 100 GHz. Gradual decrease of ε_a' and ε_c' upon cooling from 300 to 100 K is a usual behavior caused by a small phonon stiffening as a consequence of thermal contraction.

IV. DISCUSSION

The question arises about the origin of the absorption bands appearing below phonon resonances in Fig. 5. They are much weaker and significantly broader than those of polar phonons, and their strength increases when the temperature is increased, i.e., the strength is high in the paramagnetic phase. Their frequencies lying in the range of 40–100 cm^{-1} coincide with those of the magnon branch observed by INS at 7 K over the BZ[35] (see Fig. 7). In the following text we discuss whether these features can be related to the magnon dispersion branches.

Could a spin wave still exist in hexagonal $YMnO_3$ at room temperature? It is well established that Mn spins exhibit a strong short-range correlation in hexagonal $YMnO_3$ far above T_N. This was proved by an anomalous behavior of the thermal conductivity,[44] elastic moduli,[32] as well as by neutron scattering experiments.[37–39] Nevertheless, due to the short-range correlation of the spins in the hexagonal plane of $YMnO_3$, one can expect the existence of only short-wavelength paramagnons, i.e., magnons with large wave vectors $\boldsymbol{q}_x$ near the M point of the BZ. A part of such a paramagnon branch is schematically plotted in Fig. 7. Note that its frequency is lower than that of the magnon branch at 7 K, as the magnon frequency decreases by almost 10 cm^{-1} on heating toward T_N (see Fig. 2).

Electromagnons are excitations with frequencies close to those of spin waves, which, due to specific couplings, are activated in the dielectric spectra. In perovskite manganites, the parts of magnon branches exhibiting a high density of states are mainly involved in these interactions (at BZ edge or close to the spin modulation wave vector).[13] However, these electromagnons were observed only at very low temperatures (typically less than 50 K). Their strength dramatically decreases upon heating and they usually disappear from the spectra at T_N or close above T_N.[4–6] This is in contradiction with our observations in $YMnO_3$.

We came to the conclusion that the broad absorption bands we observe in the dielectric spectra reflect excitations which must be coupled to phonons. Let us discuss in brief which types of interaction between the magnetic subsystem and other degrees of freedom might be expected on the basis of the point group crystallographic symmetry $6mm$ and the magnetic symmetry $\underline{6}m\underline{m}$.[21] The magnetic order parameter of

$YMnO_3$ was analyzed in several publications and it was shown to transform following B_1 (Γ_4) irreducible representation of the $6mm$ group.[45–48] The $\underline{6}m\underline{m}$ symmetry strictly forbids the linear magnetoelectric effect, i.e., bilinear terms $\alpha_{ij}H_iE_j$ (where H_i and E_i are components of the magnetic and electric field, respectively) are not allowed in the thermodynamic potential.[22] However, a higher order magnetoelectric effect (called sometimes the magnetodielectric effect), accounted for by the $\beta_{ijk}H_iH_jE_k$ terms in the thermodynamic potential, is allowed. This effect manifests itself in our measurements as a kink near T_N in the temperature dependence of ε_a' (see Fig. 6).

The magnetic symmetry of $YMnO_3$ allows the piezomagnetic contribution to the thermodynamic potential described by the terms $p_{ijk}H_i\sigma_{jk}$, where σ_{jk} is a stress component and p_{ijk} denotes components of the piezomagnetic tensor.[22,24] We believe that this type of bilinear coupling must play an important role in the interaction between the magnetic subsystem and the lattice. Usually, the piezomagnetic effect is allowed thanks to the relativistic part of spin-lattice and spin-spin interactions, provided the symmetry restrictions are met.[25] However, in $YMnO_3$, which is a noncollinear antiferromagnet, the exchange (Coulomb) interactions may be by several orders of magnitude stronger than the relativistic ones and, therefore, they can be the origin of piezomagnetism.[49] For example, extraordinary spin-phonon interactions were shown to contribute to the thermal conductivity of $YMnO_3$ below T_N.[44] Higher order effects such as $p_{ijkl}H_iH_j\sigma_{kl}$ are naturally also allowed in $YMnO_3$.

In order to provide a more quantitative explanation of the interaction between magnetic subsystem and phonons, we calculated the phonon spectrum from first principles within the spin-polarized local density approximation.[50] We used projector augmented-wave potentials as implemented in Vienna *Ab Initio* Simulation Package (VASP).[51–54] The following valence-electron configurations were considered: $4s^24p^65s^24d^1$ for Y, $3p^64s^23d^5$ for Mn, and $2s^22p^4$ for oxygen. To account for the strong electron correlation effects on the d shells of Mn atoms, we used LDA + U approach[55,56] with an on-site Coulomb parameter $U = 8.0$ eV and Hund's exchange $J_H = 0.88$ eV as calculated in Ref. 57. The spin-orbit interaction was not taken into account. We used an A-type antiferromagnetic structure, where spins on Mn honeycomb layers are aligned ferromagnetically and the layers with opposite spin-direction alternate along the c axis.[58,59] A kinetic energy cutoff of 500 eV and a $4 \times 4 \times 2$ Γ-centered k-point mesh was used in the structural relaxation of the unit cell, where the Hellman-Feynman forces were minimized to a value smaller than 0.5 meV/Å. Phonon calculations were performed on a $2 \times 2 \times 1$ Γ-centered k-point mesh, with a $2 \times 2 \times 2$ supercell within the force-constant method.[60,61] The Hellman-Feynman forces were calculated for displacements of atoms of up to 0.04 Å. The dynamical matrix for each q point in the BZ was constructed by a Fourier transformation of the force constants, calculated for the Γ point and for the BZ boundaries. Phonon-mode frequencies and atomic displacement patterns for each q point were obtained as eigenvalues and eigenvectors of the dynamical matrices. The result for directions A-Γ-M and wave numbers up to 200 cm^{-1} are presented in Fig. 7.

As we have already pointed out, the absorption strength significantly increases upon heating. This is typical for difference frequency absorption. Such a process includes the annihilation of one quasiparticle (phonon or magnon) with frequency ω_1 and the creation of another quasiparticle with a higher frequency ω_2. The dielectric resonance then occurs at frequency $\omega_{diel} = \omega_2 - \omega_1$. This process can involve excitations from the whole BZ provided that the total wave vector is conserved. The contribution of the parts of the dispersion branch with the highest density of states is expected to dominate. The high number of available states is found namely at the flat parts of the bands close to the BZ boundaries, as it was observed, for example, in MgO.[62]

Obviously such a process is strongly temperature dependent, as it is related to the population of excitations with frequency ω_1, which follows the Bose-Einstein statistics. At low temperatures, the population of the levels which we study is close to zero and the differential absorption then practically vanishes. It becomes more probable when the energy level is thermally populated at higher temperatures. This is in qualitative agreement with our observations.

The differential transitions at the BZ boundary are possible only between phonons with the same symmetry and if the total wave vector is conserved (i.e., the transition must be vertical in the wave-vector space). The broad absorption around 90 cm^{-1} seen in ε_a spectra [Fig. 5(b)] can be explained by differential multiphonon absorption. Phonons near 60 and 150 cm^{-1} at the A point of BZ are polarized in the hexagonal plane (marked as a in Fig. 7) and their difference gives the frequency $\omega_{diel3} = 90$ cm^{-1}, as observed.

However, the two bands seen in ε_c spectra around $\omega_{diel1} =$ 40 cm^{-1} and $\omega_{diel2} = 100$ cm^{-1} are impossible to explain by multiphonon absorption. The frequency of the c-polarized phonons at the BZ edge is higher than 100 cm^{-1}. It means that the population of such phonons should be much lower than that of the a-polarized phonon at 60 cm^{-1}. For this reason, the strength of the differential multiphonon absorption in the ε_c spectra should be weaker than in ε_a spectra. Moreover, within such a hypothesis, a continuous absorption band would be expected in the spectra due to the large number of c-polarized phonons at the M point (see scheme in Fig. 7). This is in contradiction with the experimental results presented in Fig. 5.

We assume the existence of paramagnons near the M point, and in this case a differential paramagnon-phonon absorption with several maxima can be obtained. Moreover, because of the similar Bose-Einstein factor for the paramagnon close to 70 cm^{-1} and phonon near 60 cm^{-1} at the A point, the absorptions observed in both ε_a and ε_c should have comparable strengths. This fits well with the experiment. The frequency ω_{diel1} increases upon heating (Fig. 3) presumably due to the softening of the paramagnon branch with increasing temperature. The increase of the oscillator strength $\Delta\varepsilon\omega_{diel1}^2$ of the mode observed in Fig. 3 is compatible with the temperature increase of the Bose-Einstein factor: this is demonstrated by the dotted line which shows the expected population increase of an energy level at 66 cm^{-1} (i.e., the frequency of paramagnon at $\boldsymbol{q}_{BZE}$).

V. CONCLUSIONS

The THz and FTIR transmission spectra of hexagonal $YMnO_3$ clearly revealed two kinds of excitations of different

nature, which exist below polar phonon frequencies. The sharp AFM resonance band observed near 40 cm^{-1} at low temperatures broadens upon heating and disappears close to T_N. This resonance is the main contributor to the magnetic permeability μ_a. Additional broad excitations were observed in the frequency range 40–100 cm^{-1} in the dielectric permittivity spectra in both the AFM and paramagnetic phases. Our theoretical explanation of the activation of these excitations in the THz dielectric spectra is based on two-particle differential processes schematically shown in Fig. 7. The resonance observed in ε_a spectra is caused by differential phonon absorption in the A point of the BZ. The two broad absorption bands in ε_c spectra were described as differential phonon-paramagnon processes. The absorption strength of these excitations in the THz spectra increases upon heating due to the growing population of paramagnons and phonons with temperature. This is possible in the paramagnetic phase owing to strong short-range spin correlations within hexagonal planes of $YMnO_3$. The processes we observe in $YMnO_3$, where the linear magnetoelectric coupling is forbidden, are clearly different from the one responsible for the appearance of electromagnons in multiferroics with spin-induced ferroelectricity.[1,2,4,5] The multiphonon absorptions are allowed by symmetry in all dielectric systems, while paramagnon-phonon absorptions can be expected only in paramagnetic systems with a strong short-range magnetic order (e.g., in hexagonal manganites). Magnon-phonon absorption should be also detectable in all magnetically ordered systems (FM, AFM, ferrimagnets, etc.) with relatively high critical temperatures. In such conditions, the magnons at the Brillouin zone edge may become sufficiently populated to allow multiparticle effects in the spectra. This may stimulate further THz and FIR studies of other magnetically polarizable systems.

ACKNOWLEDGMENTS

The authors thank M. Mostovoy for valuable discussions. This work was supported by the Czech Science Foundation (Project No. 202/09/0682), by AVOZ10100520, and by the Young Investigators Group Program of the Helmholtz Association (Contract VH-NG-409). The contribution of Ph.D. student V.G. has been supported by Project Nos. 202/09/H041 and SVV-2011-263303. R.V.P. acknowledges the support by the RFBR (Project No. 09-02-00070). The support of the Jülich Supercomputing Center is gratefully acknowledged.

*kamba@fzu.cz

[1] A. Pimenov, A. A. Mukhin, V. Yu. Ivanov, V. D. Travkin, A. M. Balbashov, and A. Loidl, Nature Phys. **2**, 97 (2006).
[2] A. B. Sushkov, R. V. Aguilar, S. Park, S.-W. Cheong, and H. D. Drew, Phys. Rev. Lett. **98**, 027202 (2007).
[3] V. G. Bar'yakhtar and I. E. Chupis, Sov. Phys. Solid State **11**, 2628 (1970).
[4] A. Pimenov, A. M. Shuvaev, A. A. Mukhin, and A. Loidl, J. Phys. Condens. Matter **20**, 434209 (2008).
[5] N. Kida, Y. Takahashi, J. S. Lee, R. Shimano, Y. Yamasaki, Y. Kaneko, S. Miyahara, N. Furukawa, T. Arima, and Y. Tokura, J. Opt. Soc. Am. B **26**, A35 (2009).
[6] A. M. Shuvaev, A. A. Mukhin, and A. Pimenov, J. Phys. Condens. Matter **23**, 113201 (2011).
[7] N. Kida, D. Okuyama, S. Ishiwata, Y. Taguchi, R. Shimano, K. Iwasa, T. Arima, and Y. Tokura, Phys. Rev. B **80**, 220406(R) (2009).
[8] D. I. Khomskii, J. Magn. Magn. Mater. **306**, 1 (2006).
[9] D. Khomskii, Physics **2**, 20 (2009).
[10] Th. Lottermoser, D. Meier, R. V. Pisarev, and M. Fiebig, Phys. Rev. B **80**, 100101 (2009).
[11] J. S. Lee, N. Kida, S. Miyahara, Y. Takahashi, Y. Yamasaki, R. Shimano, N. Furukawa, and Y. Tokura, Phys. Rev. B **79**, 180403(R) (2009).
[12] P. Rovillain, M. Cazayous, Y. Gallais, M-A. Measson, A. Sacuto, H. Sakata, and M. Mochizuki, Phys. Rev. Lett. **107**, 027202 (2011).
[13] R. Valdés Aguilar, M. Mostovoy, A. B. Sushkov, C. L. Zhang, Y. J. Choi, S.-W. Cheong, and H. D. Drew, Phys. Rev. Lett. **102**, 047203 (2009).
[14] M. Mochizuki, N. Furukawa, and N. Nagaosa, Phys. Rev. Lett. **104**, 177206 (2010).
[15] M. Cazayous, Y. Gallais, A. Sacuto, R. de Sousa, D. Lebeugle, and D. Colson, Phys. Rev. Lett. **101**, 037601 (2008).
[16] G. Komandin, V. Torgashev, A. Volkov, O. Porodinkov, I. Spektor, and A. Bush, Phys. Solid State **52**, 734 (2010).
[17] D. Talbayev, S. A. Trugman, S. Lee, H. T. Yi, S.-W. Cheong, and A. J. Taylor, Phys. Rev. B **83**, 094403 (2011).
[18] A. S. Gibbs, K. S. Knight, and P. Lightfoot, Phys. Rev. B **83**, 094111 (2011).
[19] E. Bertaut and M. Mercier, Phys. Lett. **5**, 27 (1963).
[20] T. Chatterji, S. Ghosh, A. Singh, L. P. Regnault, and M. Rheinstädter, Phys. Rev. B **76**, 144406 (2007).
[21] M. Fiebig, D. Fröhlich, K. Kohn, St. Leute, Th. Lottermoser, V. V. Pavlov, and R. V. Pisarev, Phys. Rev. Lett. **84**, 5620 (2000).
[22] R. R. Birss, *Symmetry and Magnetism* (North-Holland, Amsterdam, 1967).
[23] M. Fiebig, Th. Lottermoser, D. Fröhlich, A. V. Goltsev, and R. V. Pisarev, Nature (London) **419**, 818 (2002).
[24] A. V. Goltsev, R. V. Pisarev, Th. Lottermoser, and M. Fiebig, Phys. Rev. Lett. **90**, 177204 (2003).
[25] L. D. Landau and E. M. Lifshitz, *Electrodynamics of Continuos Media*, 2ed. (Pergamon Press, Oxford, 1984).
[26] M. Fiebig, V. V. Pavlov, and R. V. Pisarev, J. Opt. Soc. Am. B **22**, 96 (2005).
[27] T. Choi, Y. Horibe, H. T. Yi, Y. J. Choi, Wu Weida, and S.-W. Cheong, Nat. Mater. **9**, 253 (2010).
[28] S. Lee, A. Pirogov, M. Kang, K.-H. Jang, M. Yonemura, T. Kamiyama, S.-W. Cheong, F. Gozzo, N. Shin, H. Kimura, Y. Noda, and J.-G. Park, Nature (London) **451**, 805 (2008).
[29] Y. Aikawa, T. Katsufuji, T. Arima, and K. Kato, Phys. Rev. B **71**, 184418 (2005).
[30] M. Zaghrioui, V. Ta Phuoc, R. A. Souza, and M. Gervais, Phys. Rev. B **78**, 184305 (2008).
[31] H. Fukumura, S. Matsui, H. Harima, K. Kisoda, T. Takahashi, T. Yoshimura, and N. Fujimura, J. Phys. Condens. Matter **19**, 365239 (2007).

[32]M. Poirier, F. Laliberté, and L. Pinsard, and A. Revcolevschi, Phys. Rev. B **76**, 174426 (2007).
[33]T. Penney, P. Berger, and K. Kritiyakirana, J. Appl. Phys. **40**, 1234 (1969).
[34]V. Goian, S. Kamba, C. Kadlec, D. Nuzhnyy, P. Kužel, J. Agostino Moreira, A. Almeida, and P. B. Tavares, Phase Transitions **83**, 931 (2010).
[35]T. J. Sato, S.-H. Lee, T. Katsufuji, M. Masaki, S. Park, J. R. D. Copley, and H. Takagi, Phys. Rev. B **68**, 014432 (2003).
[36]S. Petit, F. Moussa, M. Hennion, S. Pailhès, L. Pinsard-Gaudart, and A. Ivanov, Phys. Rev. Lett. **99**, 266604 (2007).
[37]J. Park, J.-G. Park, G. S. Jeon, H.-Y. Choi, Ch. Lee, W. Jo, R. Bewley, K. A. McEwen, and T. G. Perring, Phys. Rev. B **68**, 104426 (2003).
[38]B. Roessli, S. N. Gvasaliya, E. Pomjakushina, and K. Conder, JETP Lett. **51**, 287 (2005).
[39]F. Demmel and T. Chatterji, Phys. Rev. B **76**, 212402 (2007).
[40]S. Pailhès, X. Fabrèges, L. P. Régnault, L. Pinsard-Godart, I. Mirebeau, F. Moussa, M. Hennion, and S. Petit, Phys. Rev. B **79**, 134409 (2009).
[41]P. Kužel, H. Němec, F. Kadlec, and C. Kadlec, Opt. Express **18**, 15338 (2010).
[42]S. L. Dexheimer, *THz Spectroscopy: Principles and Applications* (CRC Press, Boca Raton, FL, 2008).
[43]H. Yamagichi, T. Fujita, T. Shinozaki, H. Sigie, and K. Kohn, *Ferrites: Proceedings of the Eighth International Conference on Ferrites (ICF 8)*, Kyoto and Tokyo, Japan 2000.
[44]P. A. Sharma, J. S. Ahn, N. Hur, S. Park, S. B. Kim, S. Lee, J.-G. Park, S. Guha, and S.-W. Cheong, Phys. Rev. Lett. **93**, 177202 (2004).
[45]G. M. Nedlin, Sov. Phys. Solid State **6**, 2156 (1965).
[46]Yu. G. Pashkevich, V. L. Sobolev, S. A. Fedorov, and A. V. Eremenko, Phys. Rev. B **51**, 15898 (1995).
[47]D. Sa, R. Valentí, and C. Gros, Eur. Phys. J. B **14**, 301 (2000).
[48]G. F. Koster, J. O. Dimmock, R. G. Wheeler, and H. Statz, *Properties of the Thirty Two Point Groups* (MIT Press, Cambridge, 1963).
[49]I. M. Vitebskii, N. M. Lavrinenko, and V. L. Sobolev, J. Magn. Magn. Mater. **97**, 263 (1991).
[50]J. P. Perdew and A. Zunger, Phys. Rev. B **23**, 5048 (1981).
[51]G. Kresse and J. Hafner, Phys. Rev. B **47**, 558 (1993).
[52]G. Kresse and J. Furthmüller, Phys. Rev. B **54**, 11169 (1996).
[53]P. E. Blöchl, Phys. Rev. B **50**, 17953 (1994).
[54]G. Kresse and D. Joubert, Phys. Rev. B **59**, 1758 (1999).
[55]V. I. Anisimov, F. Aryasetiawan, and A. I. Lichtenstein, J. Phys. Condens. Matter **9**, 767 (1997).
[56]S. L. Dudarev, G. A. Botton, S. Y. Savrasov, C. J. Humphreys, and A. P. Sutton, Phys. Rev. B **57**, 1505 (1998).
[57]J. E. Medvedeva, V. I. Anisimov, M. A. Korotin, O. N. Mryasov, and A. J. Freeman, J. Phys. Condens. Matter **12**, 4947 (2000).
[58]C. J. Fennie and K. M. Rabe, Phys. Rev. B **72**, 100103(R) (2005).
[59]B. B. van Aken, T. T. M. Palstra, A. Filippetti, and N. A. Spaldin, Nat. Mater. **3**, 164 (2004).
[60]D. Alfè, Comput. Phys. Commun. **180**, 2622 (2009).
[61]K. Kunc and R. M. Martin, Phys. Rev. Lett. **48**, 406 (1982).
[62]G. A. Komandin, O. E. Porodinkov, I. E. Spector, and A. A. Volkov, Phys. Solid State **51**, 2045 (2009).